Journal of Materials Chemistry C

Accepted Manuscript

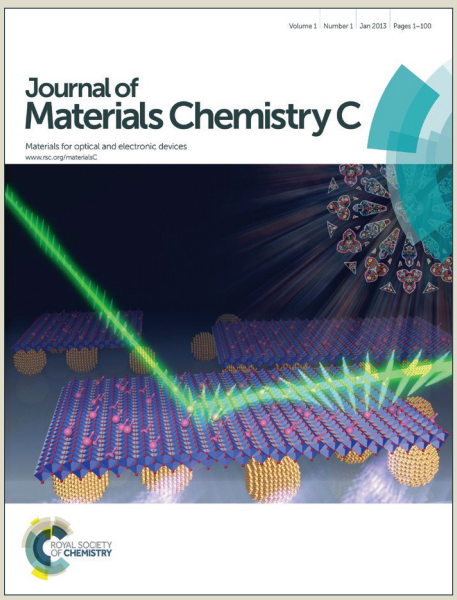

ROYAL SOCIETY OF CHEMISTRY

www.rsc.org/materialsC

Enhanced Luminescence of Mn^{4+}: $Y_3Al_5O_{12}$ Red Phosphor via Impurity Doping

Daqin Chen[*,a], Yang Zhou [a], Wei Xu [a], Jiasong Zhong [a], Zhenguo Ji [a], Weidong Xiang [*,b]

[a]College of Materials & Environmental Engineering, Hangzhou Dianzi University, Hangzhou, 310018, P. R. China
[b]College of Chemistry and Materials Engineering, Wenzhou University, Wenzhou 325035, P. R. China

Abstract Currently, Ce^{3+}: $Y_3Al_5O_{12}$ phosphor converted white light-emitting-diodes suffer from the shortage of red component and the easy aging of the organic silicone binder. Herein, a novel and non-rare-earth doped Mn^{4+}: $Y_3Al_5O_{12}$ red phosphor was synthesized by a traditional solid-state reaction. This phosphor can emit red luminescence attributed to Mn^{4+}: $^2E \rightarrow {}^4A_2$ spin-forbidden transition in the 600-700 nm spectral region and can be efficiently excited by both the commercially available near-ultraviolet and blue chips. Impressively, Mg^{2+}, Ca^{2+}, Ge^{4+} dopants were found to be beneficial to enhancing Mn^{4+} luminescence and the related mechanisms were systematically discussed. Furthermore, Mn^{4+}: $Y_3Al_5O_{12}$ embedded inorganic glass ceramic was successfully fabricated to replace phosphor in organic silicone as the color converter, and a stacking geometric configuration by sequentially coupling a Ce^{3+}: $Y_3Al_5O_{12}$ glass ceramic and a Mn^{4+}: $Y_3Al_5O_{12}$ glass ceramic with an InGaN blue chip was designed to explore its possible application in warm white light-emitting diodes.

1. Introduction

Currently, the major commercial white light-emitting diode (WLED) is the phosphor converted LED made of the InGaN blue-emitting chip and the Ce^{3+}: $Y_3Al_5O_{12}$ (Ce^{3+}: YAG) yellow phosphor dispersed in the organic silicone.[1-5] However, this strategy suffers from two major shortcomings. Firstly, the shortage of red luminescent component in the Ce^{3+}: YAG phosphor leads to high correlated color temperature (CCT) and low color rendering index (CRI) of WLED.[6,7] Furthermore, the easy aging of the organic binder ascribing to the accumulated heat emitting from the blue chip will reduce the long-term reliability and lifetime of WLED.[8,9] Therefore, red phosphors with preferable luminescent performance and strong blue absorption are highly demanded and inorganic color converters suitable to replace the phosphor in silicone (PiS) are also desired.

The seeking of red phosphors mainly focuses on the rare-earth-doped schemes so far, for instance Eu^{2+}-doped oxynitrides and nitrides. However, it is well known that most of rare earth ions are very expensive, and some rare-earth chlorides and citrates are toxic and harmful.[10,11] Therefore, considerable efforts have been devoted to the development of the non-rare-earth-based phosphors used in warm WLEDs. Among several transition metal ions, Mn^{4+}, is a suitable activator for red phosphors as the spin-forbidden $^2E \rightarrow {}^4A_2$ transition of Mn^{4+} is always located in the red spectral region.[12,13] Moreover, the cheap and easy-to-obtain manganese raw materials are beneficial to reduce the cost of red phosphors. On the other hand, a Ce^{3+}: YAG inorganic glass ceramic (GC), a kind of composite with Ce^{3+}: YAG micro-crystals distributing among

glass matrix, has been recently demonstrated to be an excellent alternative to the Ce^{3+}: YAG PiS owing to its excellent thermal resistance and easy formability. Such GC was usually fabricated by a low-temperature co-sintering technique where the Ce^{3+}: YAG commercial phosphors were thoroughly mixed with the specifically designed inorganic glass powders, and sintered at an optimal temperature to reduce the erosion of phosphors by melting glass as little as possible.[14,15]

The objective of this work is to develop a red emitting Mn^{4+}: $Y_3Al_5O_{12}$ (Mn^{4+}: YAG) phosphor and the related Mn^{4+}: YAG GC for possible application in WLEDs. Previously, optical spectroscopy of $Y_3Al_5O_{12}$:Mn^{4+} phosphors was reported.[16-18] The advancements of current work include significant improvement of luminescent efficiency of $Y_3Al_5O_{12}$:Mn^{4+} by impurity doping such as Ca^{2+}, Mg^{2+} and Ge^{4+}, and more importantly, fabrication Mn^{4+}: $Y_3Al_5O_{12}$ embedded inorganic glass ceramic to replace phosphor in organic silicone as the color converter. Notably, by combining Mn^{4+}: YAG GC and Ce^{3+}: YAG GC with the blue chip, the warm WLEDs with the improved CCTs are successfully designed.

2. Experimental details

2.1 sample preparation

A series of Mn^{4+}: YAG phosphors are synthesized by a conventional high-temperature solid-state reaction method. The starting raw materials of Y_2O_3, Al_2O_3, MnO, M (M=Li_2CO_3, Na_2CO_3, $MgCO_3$, $CaCO_3$, GeO_2) and the 2 wt% H_3BO_3 adopted as a flux were directly used without further refinement. Based on the formula of Mn^{4+}/M (x/y): $Y_3Al_{5-x-y}O_{12}$, stoichiometric amounts of raw materials were

thoroughly grounded for 30 min. After fully grinding, the samples were put into corundum crucibles and then sintered at 1400 ℃ for 4 h in air.

Mn^{4+}: YAG (or Ce^{3+}: YAG) phosphors embedded glass ceramics were prepared by a low-temperature co-sintering technique. Firstly, the precursor glass of TeO_2-ZnO-Sb_2O_3-Al_2O_3-B_2O_3-Na_2O was fabricated by a melt quenching route at 850 °C for 30 min in ambient atmosphere. Afterwards, the prepared glass was milled to powders and mixed with 5-20 wt% Mn^{4+}: YAG phosphors thoroughly and sintered at 570 °C for 20 min to form Mn^{4+}: YAG GC. Using a similar procedure, Ce^{3+}: YAG GC can also be prepared. As a comparison, phosphor-in-silicone (PiS) samples were prepared by adding 1g Ce^{3+}: YAG and 0-3.2g Mn^{4+}: YAG to the mixing silicone gels and stirred thoroughly for 30 min.

As a proof-of-concept experiment, PiS-LED device was constructed by encapsulating a PiS color converter on an InGaN-based blue LED chip; GC-LEDs were designed by coupling a Ce^{3+}: YAG GC layer and a Mn^{4+}/Mg^{2+}: YAG GC layer with the blue chip. Opaque silica gel was coated around the edge to prevent leakage of blue light.

2.2 Characterization

Structures of these samples were investigated by power X-ray diffraction (XRD) analysis on a Bruker D8 diffractometer with CuKa radiation operating at 40 kV and 40 mA. Microstructures of the GC samples were studied using a scanning electron microscope (SEM; JSM-6700F, JEOL, Ltd., Tokyo, Japan) equipped with an energy dispersive X-ray spectroscopy (EDS) system. Emission, excitation spectra and Mn^{4+}

decay curves were recorded on an Edinburgh Instruments (Edinburgh, UK) FS5 spectrofluorometer equipped with both continuous (150 W) and pulsed xenon lamps. Temperature-dependent emission spectra of the red phosphor were recorded on the Edinburgh Instruments FS5 spectrofluorometer equipped with a homemade temperature controlling stage. Luminous efficacy, Chromaticity coordinate, CCT and CRI of the WLEDs were measured in a HAAS-2000 spectroradiometer equipped with an integrating sphere of 50 cm diameter (Everfine Corporation, Hangzhou, China). The current for exciting the blue chip was fixed at 60 mA. Quantum yield (QY), defined as the ratio of the emitted photons to the absorbed photons, is determined according to the following expression[15]

$$\eta = \frac{number\ of\ photons\ emitted}{number\ of\ photons\ absorbed} = \frac{L_{sample}}{E_{reference} - E_{sample}} \qquad (1)$$

where η represents QY, L_{sample} the emission intensity, $E_{reference}$ and E_{sample} the intensities of the excitation light not absorbed by the reference and the sample respectively. The measurements were carried out on a spectrofluoremeter (FS5) equipped with an integrating sphere.

3. Results and discussion

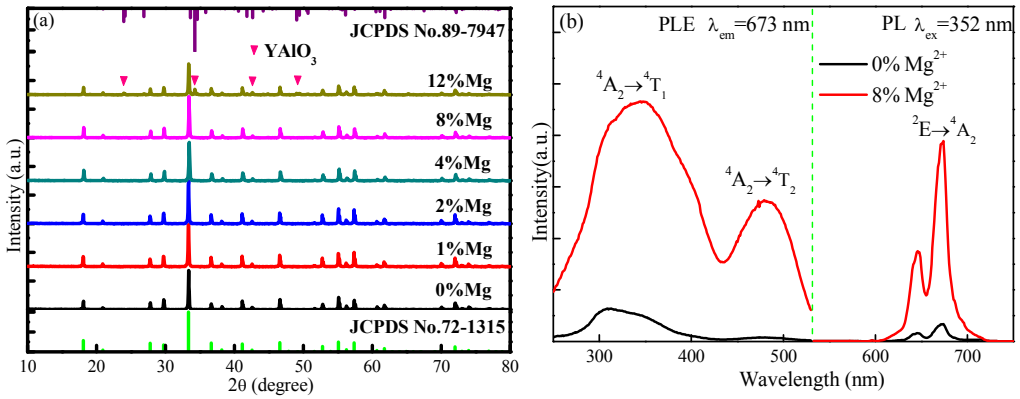

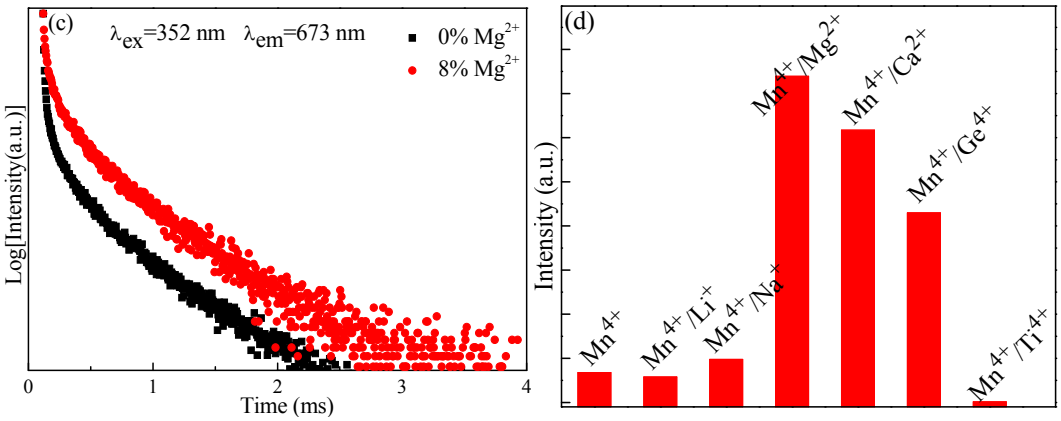

Fig. 1 (a) XRD patterns of Mn^{4+}/Mg^{2+} (0.1/y mol%): YAG (y=0, 1, 2, 4, 8, 12) phosphors; bars represent standard $Y_3Al_5O_{12}$ (JCPDS No. 72-1315) and $YAlO_3$ (JCPDS No. 33-0041) crystal data. (b) PLE (λ_{em}=673 nm) and PL (λ_{em}=352 nm) spectra of Mn^{4+} (0.1 mol%): YAG and Mn^{4+}/Mg^{2+} (0.1 mol%/8 mol%): YAG. (c) Decay curves of Mn^{4+}: ^2E excited state (λ_{em}=673 nm) with and without Mg^{2+} doping. (d) Integrated intensity for the Mn^{4+} (0.1 mol%): YAG and Mn^{4+}/M (0.1/8 mol%): YAG (M=Li^+, Na^+, Mg^{2+}, Ca^{2+}, Ge^{4+}, Ti^{4+}) phosphors.

XRD patterns of Mn^{4+}/Mg^{2+}(x/y, mol%): $Y_3Al_{5-x-y}O_{14}$ (x=0.1; y=0, 1, 2, 4, 8, 12) phosphors are shown in Figure 1a. With increase of Mg^{2+} content from 0 to 8 mol%, XRD patterns of phosphors agree well with that of standard $Y_3Al_5O_{12}$ (JCPDS No. 72-1315). Further increment of Mg^{2+} content will induce an extra impurity phase of $YAlO_3$ (JCPDS No. 33-0041). Similarly, Mn^{4+}/M: $Y_3Al_5O_{12}$ (M=Na^+, Ca^{2+}, Ge^{4+}) (Mn^{4+}/M: YAG) phosphors show a maximal M content of 8 mol% (Figure S1-S3). Photoluminescence (PL) and PL excitation (PLE) spectra of Mn^{4+} (0.1 mol%): YAG and Mn^{4+}/Mg^{2+}: (0.1/8 mol%) YAG phosphors are presented in Figure 1b. The emission and excitation bands of Mn^{4+}/Mg^{2+}: YAG are located at the same wavelengths as those of Mn^{4+}: YAG, indicating that the addition of Mg^{2+} has no obvious impact on crystal structure of YAG. PL spectra show two emission bands centered at 646 and 673 nm, which are due to the spin-forbidden $^2E \rightarrow {}^4A_2$ transition of Mn^{4+}. PLE spectra monitored at 673 nm emission consist of two strong excitation peaks centered at 345 and 480 nm, respectively, which are assigned to $^4A_2 \rightarrow {}^4T_1$ and

$^4A_2 \rightarrow {}^4T_2$ transitions of Mn^{4+}.[19,20] As evidenced in Figure 1b, Mg^{2+} dopants significantly enhance the emission intensity of Mn^{4+}: YAG, which is further confirmed by decay curves of Mn^{4+} (Figure 1c). Figure 1d depicts the effects of Li^+, Na^+, Mg^{2+}, Ca^{2+}, Ge^{4+} and Ti^{4+} dopants on the emission intensities of Mn^{4+}: YAG. Therein, Mg^{2+}, Ca^{2+} and Ge^{4+} have the ability to enhance luminescence of Mn^{4+}: YAG phosphor, Li^+ and Na^+ have not obvious impact on Mn^{4+}: YAG luminescence, and the Ti^{4+} doped Mn^{4+}: YAG phosphor shows no luminescence under UV or blue light excitation. Specifically, quantum yields of Mn^{4+}: YAG phosphors with and without 8mol% Mg^{2+} doping were measured to be about 6.3 and 48.6%, respectively, supporting the conclusion that Mn^{4+}: YAG luminescence can be greatly enhanced via impurity doping.

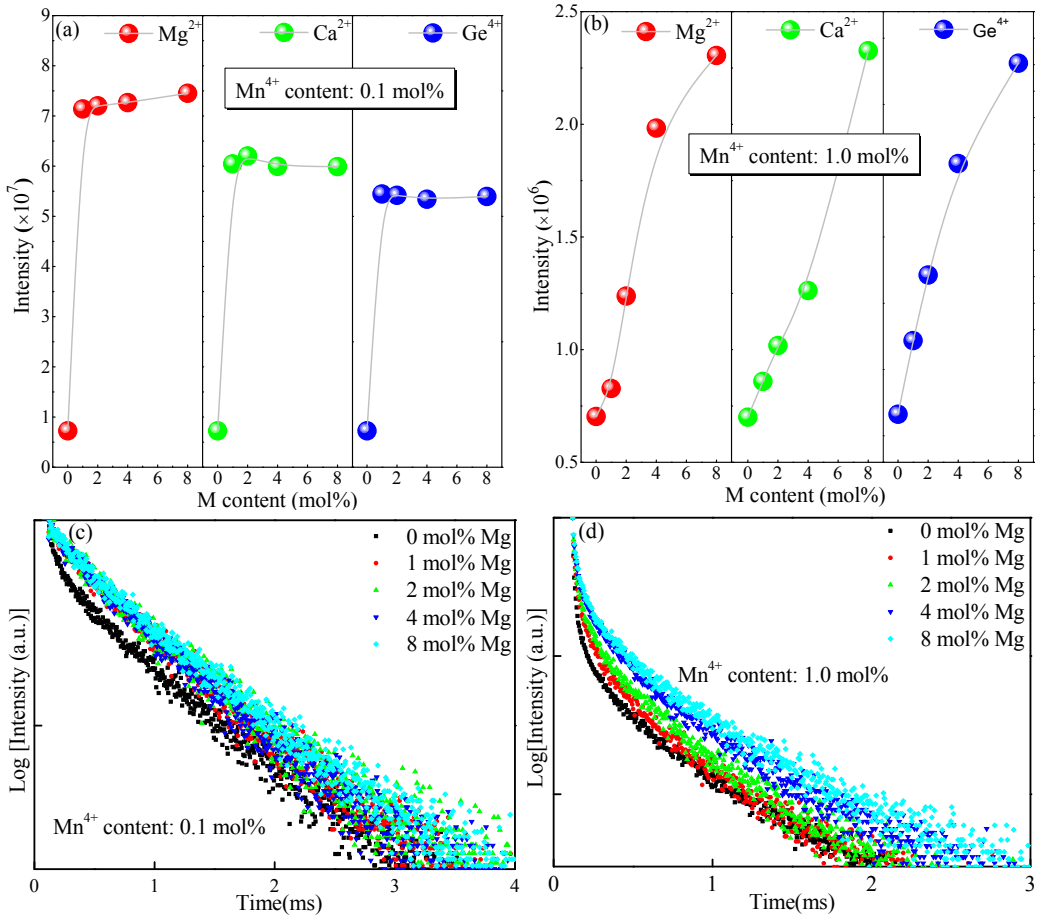

Fig. 2 Dependence of Mn^{4+} PL intensity on co-dopant concentration for (a) Mn^{4+}/M (0.1/y mol%): YAG (M=Mg, Ca, Ge; y=0, 2, 4, 6, 8) and (b) 1.0 mol% Mn^{4+}/ y mol% M: YAG (M=Mg, Ca, Ge; y=0, 2, 4, 6, 8) phosphors. Decay curves of Mn^{4+}: ^2E excited state (λ_{em}=673 nm) in (c) Mn^{4+}/Mg^{2+}(0.1/y mol%): YAG and (d) Mn^{4+}/Mg^{2+} (1.0/y mol%): YAG (y=0, 2, 4, 6, 8) under 352 nm UV light excitation.

The dependence of integrated PL intensity I_{PL} of Mn^{4+} (x mol%): YAG (x=0.1, 1.0) on Mg^{2+}, Ca^{2+} and Ge^{4+} doping content (y=0~8 mol%) is provided in Figure 2. When Mn^{4+} concentration is fixed to 0.1 mol%, I_{PL} is not obviously altered for y≥1%, but significantly increases comparing to Mn^{4+}: YAG without Mg^{2+}, Ca^{2+} and Ge^{4+} doping, as shown in Figure 2a; when Mn^{4+} concentration is fixed to 1 mol%, I_{PL} monotonously enhances with increase of the Mg^{2+}, Ca^{2+} and Ge^{4+} doping content (Figure 2b). These experimental results suggest that Mn^{4+} luminescence in YAG host is highly sensitive to the content of Mn^{4+} activators and $Mg^{2+}/Ca^{2+}/Ge^{4+}$ co-dopants. In order to further verify the role of co-doping ions on enhancing Mn^{4+} luminescence, the corresponding decay behaviors of these Mn^{4+}/Mg^{2+} (x/y mol%): YAG (x=0.1, 1.0; y=0, 1, 2, 4, 8) phosphors were investigated, as shown in Figure 2c and 2d. The corresponding lifetimes were evaluated via the equation of $\tau = \int I(t)dt / I_p$ because of non-single-exponential characteristics of these decay curves, where I_p is the peak intensity and *I(t)* is the time-related luminescence intensity. Obviously, the trend of lifetime variation is consistent with that of PL intensity variation. For x=0.1 mol%, the lifetime of Mn^{4+} in phosphor with the addition of co-doping ions becomes longer, and reaches saturation when y≥1% (Figure 2c). However, for x=1.0 mol%, the lifetime of Mn^{4+} gradually increases with increase of co-dopant concentration (Figure 2d). Notably, similar decay behaviors can be found in Ca^{2+} and Ge^{4+} co-doped Mn^{4+}: YAG phosphors (Figure S4, S5).

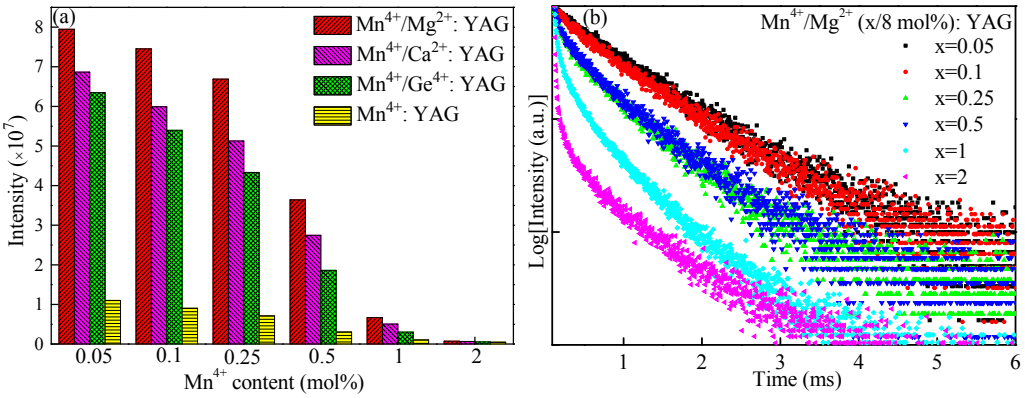

Fig. 3 (a) Relationship between Mn^{4+} content and PL intensity of Mn^{4+}/M (x/8 mol%): YAG (M= Mg^{2+}, Ca^{2+}, Ge^{4+}; x=0.05, 0.1, 0.25, 0.5, 1, 2) phosphors. (b) Mn^{4+} content dependent decay curves of Mn^{4+}: ^2E state (λ_{em}= 673 nm) in Mn^{4+}/Mg^{2+}: YAG under 352 nm light excitation.

In a further experiment, the influence of Mn^{4+} content on the luminescence of Mn^{4+}/M (x/8 mol%): YAG (x=0.05, 0.1, 0.25, 0.5, 1, 2; M= Mg^{2+}, Ca^{2+}, Ge^{4+}) was studied, as shown in Figure 3a. As Mn^{4+} concentration increases, the PL intensity diminishes gradually and the maximum emission intensity appears at x=0.05%. Considering that this Mn^{4+} content in YAG phosphor is quite low, it is not necessary to synthesize the phosphor with Mn^{4+} content lower than 0.05 mol%. Increasing Mn^{4+} content will monotonously reduce the emission intensity, ascribing to concentration quenching of Mn^{4+} in the YAG crystal lattice. Notably, Mg^{2+}, Ca^{2+} and Ge^{4+} co-dopants cannot change this variation tendency; however, the emission intensity is far higher than the corresponding Mn^{4+} single-doped sample. Moreover, the effect of co-dopants for improving Mn^{4+} luminescence always follows the order of Mg^{2+}>Ca^{2+}>Ge^{4+}. Likewise, the decay curves were measured to verify this phenomenon. As shown in Figure 3b, the lifetime of Mn^{4+}/Mg^{2+} (x/8 mol%): YAG (x=0.05~2) shows a considerable decrease with increase of Mn^{4+} content. Similar decay results can be found in the Mn^{4+}: YAG, Mn^{4+}/Ca^{2+}: YAG and Mn^{4+}/Ge^{4+}: YAG samples (Figure S6-S8). Figure 4 shows the luminescent photographs of the Mn^{4+}:

YAG samples co-doped with various Mg^{2+}, Ca^{2+} and Ge^{4+} contents (1~8 mol%). Under UV light excitation, the red light enhances with increase of $Mg^{2+}/Ca^{2+}/Ge^{4+}$ content (Figure 4a, 4b). Increasing Mn^{4+} content will induce a decrease of red luminescence, however, the luminescence of the corresponding Mn^{4+}/M: YAG (M=Mg^{2+}, Ca^{2+}, Ge^{4+}) is always brighter than that of the Mn^{4+} single-doped phosphors (Figure 4c).

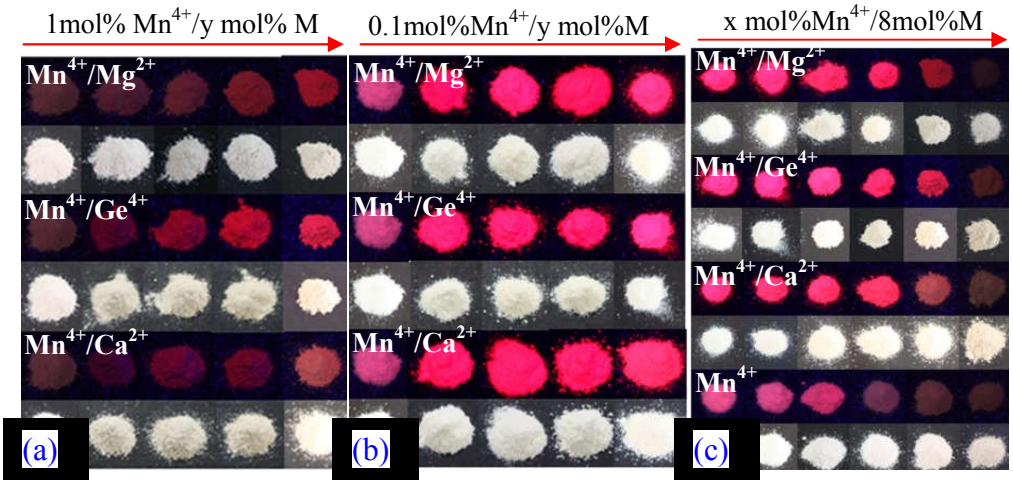

Fig. 4 Photographs of the Mn^{4+}: YAG phosphors under natural light and 352 nm UV light illumination: (a) Mn^{4+}/M (1.0/y mol%): YAG, (b) Mn^{4+}/M (0.1/y mol%): YAG (M=Mg^{2+}, Ge^{4+}, Ca^{2+}; y=1, 2, 4, 6, 8), and (c) Mn^{4+}/M (x/8 mol%): YAG (x=0.05, 0.1, 0.25, 0.5, 1, 2).

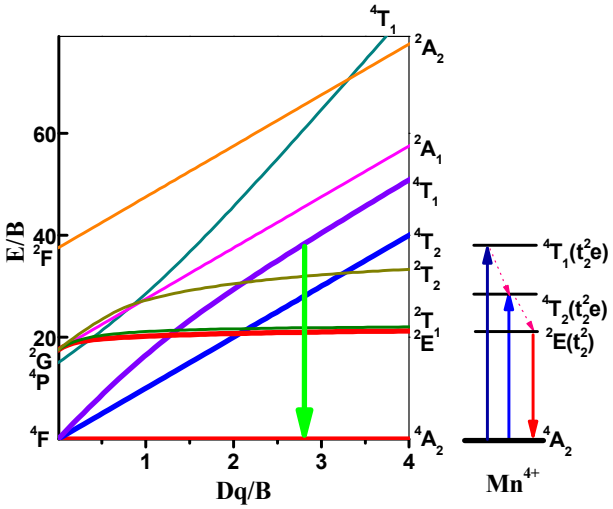

Fig. 5 Tanabe-Sugano energy-level diagram of Mn^{4+} in the YAG host.

Generally, Mn^{4+} luminescence is highly related to the crystal field strength and site symmetry of the host owing to the strong coupling of Mn^{4+} 3d electrons to lattice

vibration. Usually, the level scheme for Mn^{4+} in the host can be described using the Tanabe-Sugano diagram, as shown in Figure 5. The local crystal-field strength *Dq* can be determined by the mean peak energy (20747 cm^{-1}) of the $^4A_{2g}\rightarrow{}^4T_{2g}$ transition according to the following equation

$$Dq = \frac{E(^4T_{2g} - {}^4A_{2g})}{10} \quad (1)$$

On the basis of the peak energy difference (9556 cm^{-1}) between the $^4A_{2g}\rightarrow{}^4T_{2g}$ and $^4A_{2g}\rightarrow{}^4T_{1g}$ transitions, the Racah parameter *B* can be evaluated from the expression[2,21]

$$\frac{Dq}{B} = \frac{15(x-8)}{x^2 - 10x} \quad (2)$$

where the parameter *x* is defined as

$$x = \frac{E(^4A_{2g}\rightarrow{}^4T_{1g}) - E(^4A_{2g}\rightarrow{}^4T_{2g})}{Dq} \quad (3)$$

According to the peak energy of $^2E_g\rightarrow{}^4A_{2g}$ (14859 cm^{-1}) derived from the emission spectrum, the Racah parameter *C* can be calculated by the expression

$$E(^2E_g - {}^4A_{2g})/B = 3.05C/B + 7.9 - 1.8B/Dq \quad (4)$$

From equations (1)-(4), the crystal field parameters of *Dq*, *B*, *C* were calculated to be 2075, 1012 and 2542 cm^{-1}, respectively.

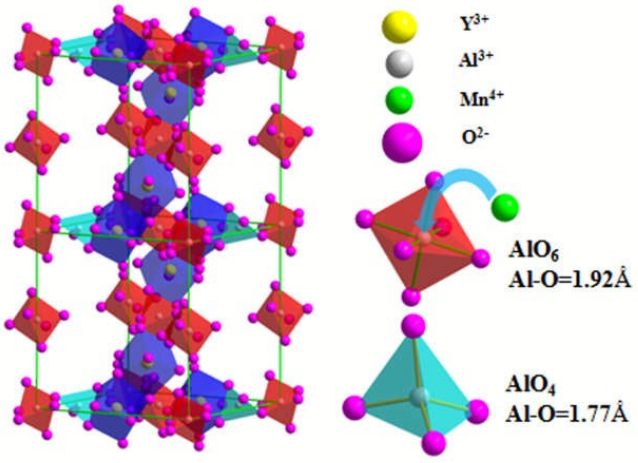

Fig. 6 Cell structure of Mn^{4+}: YAG: grey spheres represent Al^{3+} on tetrahedral and octahedral sites, and green spheres stand for Mn^{4+} ions substituting for Al^{3+} which are on octahedral sites. The Al-O distances in AlO_4 tetrahedron and AlO_6 octahedron are also provided.

$Y_3Al_5O_{12}$ crystal exhibits a cubic structure with a space group of $I_{a\text{-}3d}$ and the lattice parameters of $a=b=c$=12.010 Å, and is composed of 4- and 6-fold coordinated Al^{3+} ions and 8-fold coordinated Y^{3+} ions,[5] as shown in Figure 6. The Mn^{4+} activators prefer to occupy octahedral site of Al^{3+} in YAG host because of the approximate ionic radii between Al^{3+} (r= 0.535 Å, CN=6) and Mn^{4+} (r=0.530 Å, CN=6) and the strong ligand-field stabilization energy of Mn^{4+} in the 6-fold coordination.[21-23] Unfortunately, charge compensations are required due to the different valence between Al^{3+} and Mn^{4+} ions. Generally, O^{2-} ions are available as the interstitial impurities to realize charge balance via formation of Mn^{4+}-Mn^{4+}-O^{2-} pairs, as schematically illustrated in Figure 7a. An increase of Mn^{4+} content would significantly reduce the average distance between Mn^{4+} ions, which significantly reduces Mn^{4+} luminescence by energy migration from Mn^{4+} to O^{2-} quenching centers.

Ge^{4+} co-dopants could easily replace Al^{3+} ions because of similar ionic radii between Al^{3+} (r=0.53 Å, CN=6) and Ge^{4+} (r=0.54 Å, CN=6). As shown in Figure 7a, with the addition of Ge^{4+}, one of Mn^{4+} ions in the Mn^{4+}-Mn^{4+}-O^{2-} will be substituted by Ge^{4+}, which induces the formation of Ge^{4+}-Mn^{4+}-O^{2-} pairs. The existence of Ge^{4+} ions will interrupt the probability of energy transfer among Mn^{4+} ions and result in the enhancement of Mn^{4+} luminescence.[24] Unlike Mg^{2+} and Ge^{4+}, Ca^{2+} dopants tend to occupy Y^{3+} sites in YAG host as the ionic radii of Ca^{2+} (r=1.00 Å, CN=6) are much larger than that of Al^{3+} (r=0.53 Å, CN=6) but approximate to that of Y^{3+} (r=0.90 Å, CN=6). The possible mechanism for luminescence enhancement induced by Ca^{2+}

dopants is provided in Figure 7b. The formation of Ca^{2+}-Ca^{2+} pairs by substituting Y^{3+}-Y^{3+} pairs is beneficial to compensating charge imbalance resulted from the formation of Mn^{4+}-Mn^{4+} pairs by substituting Al^{3+}-Al^{3+} pairs. Consequently, the quenching centers are greatly reduced since no extra O^{2-} defect is required. [25]

Mg^{2+} co-dopants have a tendency to occupy both Al^{3+} and Y^{3+} sites because the ionic radius of Mg^{2+} (r=0.72 Å, CN=6) is between those of Al^{3+} (r=0.53 Å, CN=6) and Y^{3+} (r=0.90 Å, CN=6). Similar to the case of Ca^{2+} dopants, Mg^{2+}-Mg^{2+} pairs will be formed to replace Y^{3+}-Y^{3+} pairs for charge compensation (Figure 7c). More importantly, Mn^{4+}–Mg^{2+} pairs can also be produced to substitute Al^{3+}-Al^{3+} pairs without the requirement of charge compensation and additional oxygen ions when Mn^{4+} activators are doped into YAG host,[6,10,26] as shown in Figure 7c. Therefore, the existence of Mn^{4+}–Mg^{2+} pairs eliminates charge imbalance and importantly the energy migration among Mn^{4+} ions will be suppressed by Mg^{2+}, which greatly increase radiative transition probability of Mn^{4+} in the excited state.[10,26] Mg^{2+} dopants-induced enhancement of Mn^{4+} luminescence and elongation of Mn^{4+} lifetime clearly evidence the local environmental variation of Mn^{4+} in YAG host.[27,28]

Notably, Mg^{2+} ions are found to be the most efficient dopants to improve Mn^{4+} luminescence since they can not only act as charge compensating centers but also suppress the adverse energy migration among neighboring Mn^{4+} ions. Nevertheless, the Ge^{4+} and Ca^{2+} dopants only serve as cutting centers of energy migration and charge compensating ions, respectively. This leads to relatively less efficient enhancement of Mn^{4+} luminescence induced by Ge^{4+} and Ca^{2+} than Mg^{2+}.

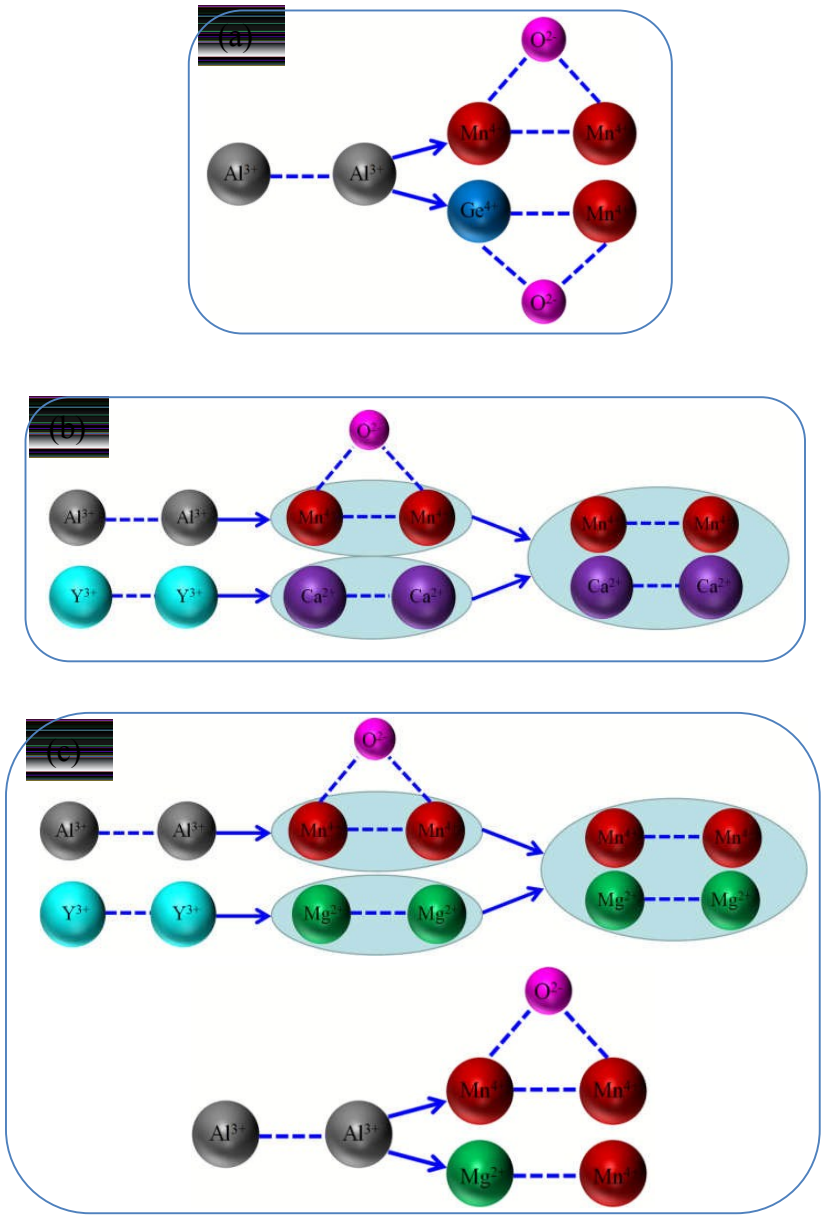

Fig. 7 (a) Mechanism of decrease concentration quenching in YAG: Mn^{4+} with Ge^{4+} doping. (b) Mechanism of charge compensation in Mn: YAG with Ca^{2+} doping. (c) Schematic illustration of the proposed mechanisms Mn^{4+}–Mn^{4+} pairs in connection with interstitial O^{2-} are transformed into Mn^{4+}–Mn^{4+} pairs without interstitial O^{2-} and isolated Mn^{4+} ions with Mg^{2+} doping.

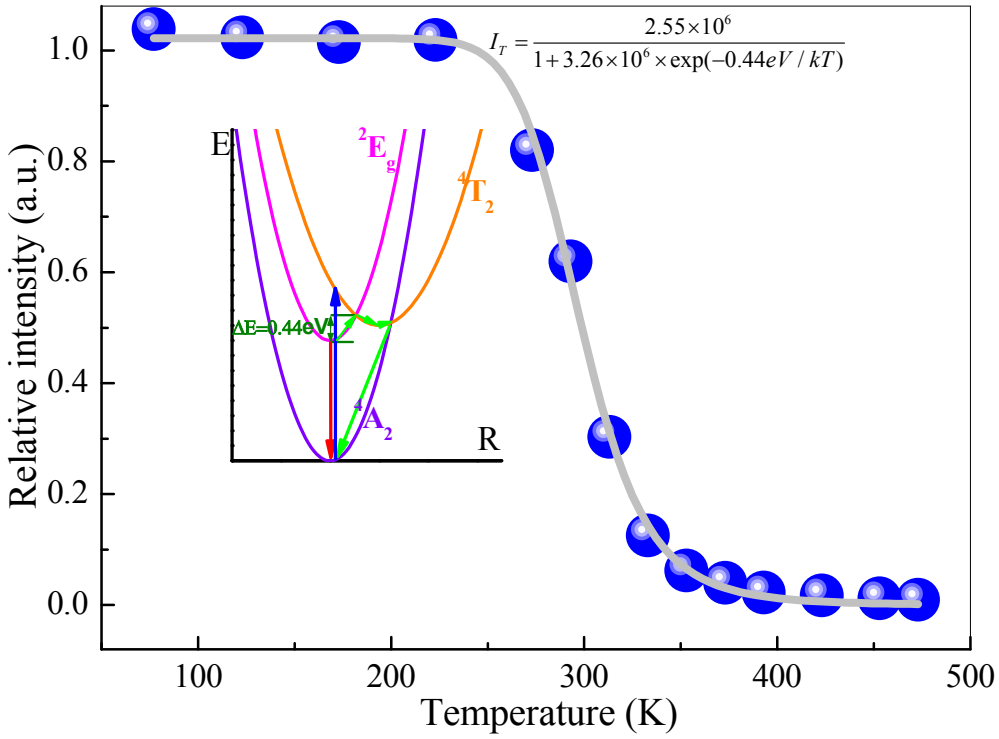

Fig. 8 Temperature dependence of PL relative intensity of Mn^{4+} ^2E_g-$^4A_2$ transition in the Mn^{4+}/Mg^{2+}: (0.1/8 mol%) YAG phosphor. Solid line represents the fitting result. Inset is the configurational coordinate diagram of Mn^{4+} in YAG host, showing the possible thermal quenching process.

The thermal quenching behavior of Mn^{4+}/Mg^{2+} (0.1/8 mol%): YAG was investigated to evaluate its potential application in WLED, as shown in Figure 8. With increase of heating temperature from 110 K to 473 K, the emission intensity gradually weakens, which can be explained by thermal quenching in the configurational coordinate diagram (inset of Figure 8). The thermal quenching activation energy is usually expressed by the following equation[29-32]

$$I_T = \frac{I_0}{1+c\times\exp(-E_a/kT)} \qquad (5)$$

where I_0 and I_T is the initial emission intensity and the luminescent intensity at temperature T, respectively, c is a constant, E_a is the activation energy and k is Boltzmann constant. The experimental data are well-fitted by Eq. 5, as demonstrated

in Figure 8, which determines the activation energy of Mn^{4+} in YAG host to be 0.44 eV.

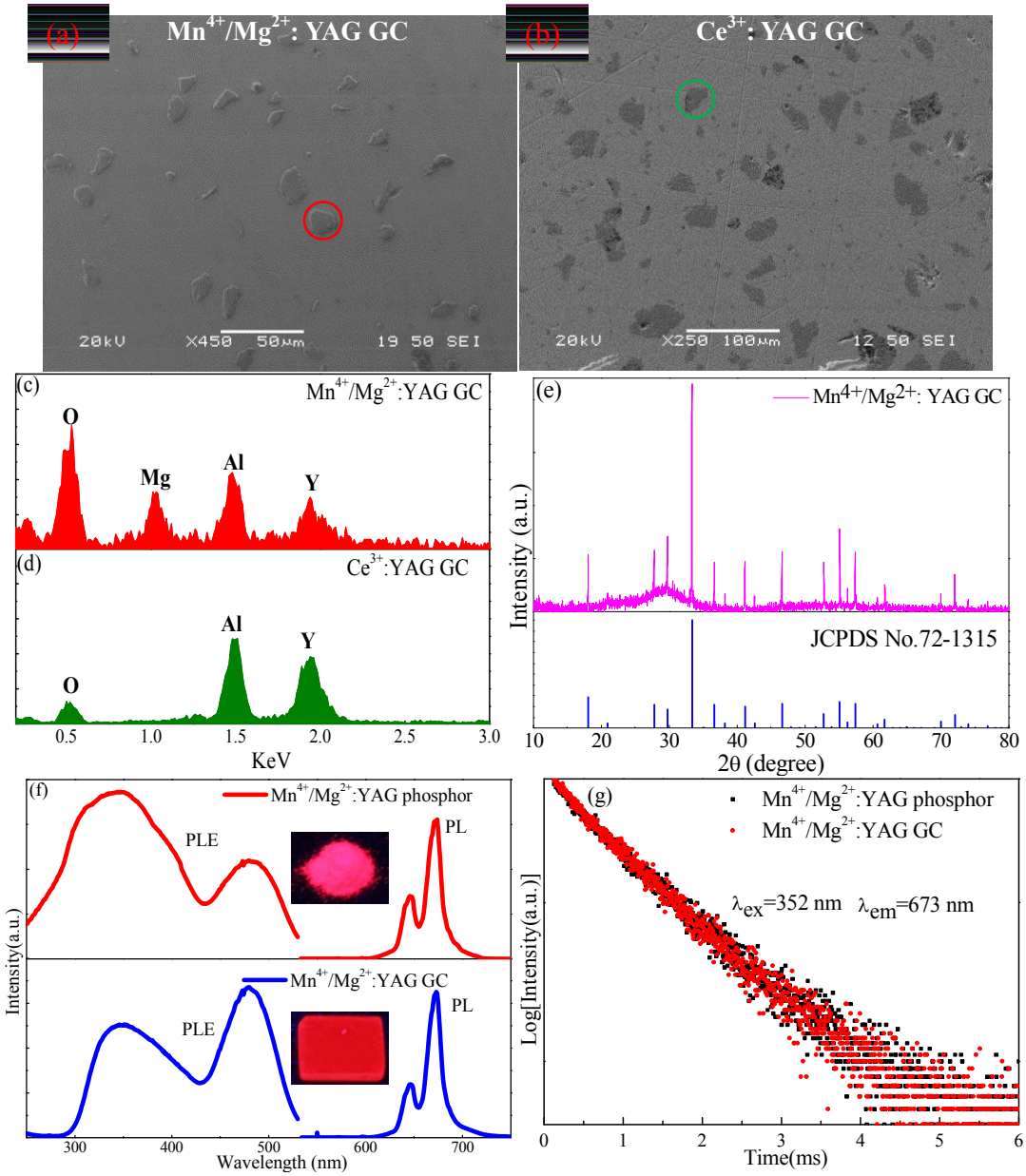

Fig. 9 SEM image of (a) Mn^{4+}/Mg^{2+} (0.1/8 mol%): YAG GC and (b) Ce^{3+} (0.5 mol%): YAG GC as well as the corresponding EDS spectra of an individual (c) Mn^{4+}/Mg^{2+}: YAG particle and (d) Ce^{3+}: YAG particle among glass matrix. (e) XRD pattern of Mn^{4+}/Mg^{2+}: YAG GC; bars represent standard cubic $Y_3Al_5O_{12}$ crystal data (JCPDS No. 72-1315). (f) PLE (λ_{em}=673 nm) and PL (λ_{em}=352 nm) spectra of the Mn^{4+}/ Mg^{2+} (0.1/8, mol%): YAG phosphor and the corresponding GC; insets are the luminescent photographs. (g) Decay curves of Mn^{4+}: ^2E excited state in the Mn^{4+}/Mg^{2+}(0.1/8, mol%): YAG phosphor and the corresponding GC.

Furthermore, both Mn^{4+}/Mg^{2+}: YAG GC and Ce^{3+}: YAG GC samples were successfully fabricated by mixing the corresponding red and yellow phosphors with

the special designed TeO_2-based glass via a low-temperature route. SEM observations on these GC samples evidently confirm that the Mn^{4+}/Mg^{2+}: YAG particles and Ce^{3+}: YAG ones sized 10–20 um are homogeneously dispersed in the glass matrix (Figure 9a, 9b). Evidently, EDS spectra (Figure 9c, 9d), performed on an individual Mn^{4+}/Mg^{2+}: YAG particle and Ce^{3+}: YAG particle among glass matrix, verify the existence of Mg/Y/Al/O and Y/Al/O elements in these two particles, respectively. Mn and Ce signals are not detectable owing to the low doping content. As revealed in Figure 9e, XRD pattern of Mn^{4+}/Mg^{2+}: YAG GC further confirmed that these particles embedded among glass matrix are Mn^{4+}/Mg^{2+}: YAG red phosphors. As expected, the excitation/emission spectrum (Figure 9f) and luminescent decay behaviors (Figure 9g) of Mn^{4+}/Mg^{2+}: YAG GC are similar to those of Mn^{4+}/Mg^{2+}: YAG powder sample. Notably, the 345 nm excitation band intensity of Mn^{4+}: YAG glass ceramic is weaker than that of Mn^{4+}: YAG phosphor, which is ascribed to the absorption of glass matrix in the short wavelength range.

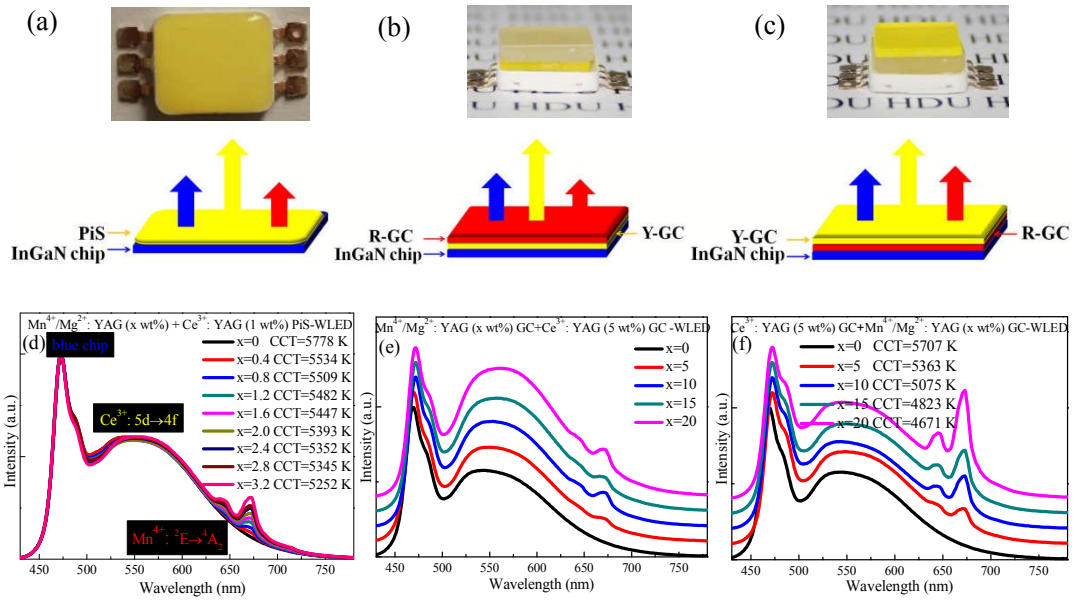

Fig. 10 Photographs of (a) PiS-LED constructed by coating a PiS layer on an InGaN-based blue

chip, (b) stacking structure of RY-GC-LED and (c) YR-GC-LED fabricated by coupling Ce^{3+}: YAG GC (Y-GC) and Mn^{4+}/Mg^{2+}: YAG GC (R-GC) with an InGaN-based blue chip. EL spectra of (d) PiS-LED, (e) RY-LED and (f) YR-LED with various Mn^{4+}/Mg^{2+}: YAG contents.

As a proof-of-concept experiment, the WLED devices were constructed by encapsulating PiS and GC color converters directly on the blue chip. As shown in Figure 10a, WLED was firstly fabricated by coating a Mn^{4+}/Mg^{2+}: YAG and Ce^{3+}: YAG co-doped PiS layer on an InGaN-based blue LED chip (PiS-LED). As demonstrated in Figure 10d, the electroluminescence (EL) spectrum of PiS-LED clearly shows a blue emission band originating from the InGaN-based chip, a broad yellow band corresponding to Ce^{3+}: 5d→4f transition of Ce^{3+}: YAG phosphor and two red emission peaks ascribing to Mn^{4+}: $^2E \rightarrow {}^4A_2$ transition of Mn^{4+}/Mg^{2+}: YAG phosphor. As the Mn^{4+}/Mg^{2+}: YAG content increases, red luminescence monotonously intensifies, and subsequently the CCT of PiS-LED decreases from 5778 K to 5252 K. Unfortunately, the increase of red luminescence and the decrease of CCT are not notable owing to the strong absorption of blue excitation light by Ce^{3+}: YAG and the opaque of PiS color converter.

As an alternative, a Ce^{3+}: YAG GC layer and a Mn^{4+}/Mg^{2+}: YAG GC layer were placed on an InGaN-based blue LED chip to construct WLED.[33] Firstly, the influence of stacking orders of Ce^{3+}: YAG GC and Mn^{4+}: YAG GC on the electroluminescent (EL) performance of GC-LEDs was examined. The configurations by placing Ce^{3+}: YAG GC adjacent to the chip (denoted as RY-GC-LED) and placing Mn^{4+}/Mg^{2+}: YAG close to the chip (denoted as YR-GC-LED) are schematically illustrated in Figure 10b and10c, respectively. The corresponding EL spectra of RY-GC-LEDs and YR-GC-LEDs were exhibited in Figure 10e and 10f, respectively. When the Ce^{3+}:

YAG yellow phosphor content in GC is fixed to 5 wt% and the Mn^{4+}/Mg^{2+}: YAG red phosphor content in GC increases from 0 to 20 wt%, red luminescence enhances gradually in both RY-GC-LEDs and YR-GC-LEDs. However, their spectra profiles are quite different, i.e., the YR-GC-LEDs emit more red light than the RY-GC-LEDs (Figure 10e, 10f). Mn^{4+} luminescence was great suppressed for RY-GC-LEDs as most blue excitation lights were absorbed by Ce^{3+}: YAG GC. On the contrary, the blue excitation lights will be firstly absorbed by Mn^{4+}/Mg^{2+}: YAG GC for YR-GC-LEDs. As Mn^{4+}/Mg^{2+}: YAG content increases in GC sample, the CCT of YR-GC-LEDs reduces from 5707 K to 4671 K. The variation of CCT for YR-GC-LEDs is apparently superior to PiS-WLED, which indicates the potential use of the stacking geometric configuration of GC for warm WLEDs.

4. Conclusions

In summary, a series of $Mg^{2+}/Ge^{4+}/Ca^{2+}$ doped Mn^{4+}: YAG red phosphors were prepared by a high-temperature solid-state reaction. These phosphors could be effectively excited by commercially available blue chip and emit bright red luminescence centered at ~673 nm. Mg^{2+}, Ge^{4+} and Ca^{2+} dopants can substitute Y^{3+}/Al^{3+}, Al^{3+} and Y^{3+} ions in the YAG host, respectively, and significantly enhance Mn^{4+} emission intensity as they can act as charge compensating ions to reduce O^{2-} quenching centers and/or interrupting ions to suppress adverse energy migration among neighboring Mn^{4+} activators. To evaluate the suitability of the investigated phosphors as red converter, Mn^{4+}/Mg^{2+}: YAG glass ceramic, in which Mn^{4+}/Mg^{2+}: YAG red phosphors were successfully incorporated into the glass host without

obviously affecting their optical performance, was further fabricated and evidenced by XRD, SEM and optical spectroscopy measurements. Finally, GC-based WLEDs were designed using a stacking geometric configuration of Ce^{3+}: YAG GC-Mn^{4+}/Mg^{2+}: YAG GC-blue chip to demonstrate the tunability of correlated color temperature by simply modifying Mn^{4+}/Mg^{2+}: YAG content. It is expected that the present Mn^{4+}/Mg^{2+}: YAG red phosphors and the corresponding GCs may find potential applications in the high-power warm WLEDs.

Author information

Corresponding Author

*E-Mail: dqchen@hdu.edu.cn (D. Q. Chen); xiangweidong001@126.com (W. D. Xiang)

Acknowledgements

This work was supported by the Natural Science Foundation of Zhejiang Province for Distinguished Young Scholars (LR15E020001), National Natural Science Foundation of China (21271170, 51372172, 61372025 and 51572065) and the 151 talent's projects in the second level of Zhejiang Province.

References

1 P. Pust and P. J. Schmidt, W. Schnick, *Nat. Mater.,* 2015, **14**, 454.

2 H. M. Zhu, C. C. Lin, W. Q. Luo, S. T. Shu, Z. Liu, Y. S. Liu, J. T. Kong, E. Ma, Y. G. Cao, R. S. Liu and X. Y. Chen, *Nat. Commun.,* 2014, **5**, 4312.

3 X. Y. Jiang, Y. X. Pan, S. M. Huang, X. A. Chen, J. G. Wang and G. K. Liu, *J. Mater. Chem. C,* 2014, **2**, 2301.

4 X. Y. Jiang, Z. Chen, S. M. Huang, J. G. Wang and Y. X. Pan, *Dalton Trans.,* 2014, **43**, 9414.

5 Z. G. Xia, C. Ma, M. S. Molokeev, Q. Liu, K. Rickert and K. R. Poepperlmeier, *J. Am. Chem. Soc.,* 2015, **137**, 12494.

6 M. M. Shang, J. Fan, H. Z. Lian, Y. Zhang, D. L. Geng and J. Lin, *Inorg. Chem.,* 2014, **53** (14), 7748.

7 W. Lu, W. Z. Lv, Q. Zhao, M. M. Jiao, B. Q. Shao and H. P. You, *Inorg. Chem.,* 2014, **53**, 11985.

8 X. Zhang, L. Huang, F. Pan, M. Wu, J. Wang and Y. Chen, Q. Su, *ACS Appl. Mater. Interfaces*, 2014, **6**, 2709.

9 X. Zhang, J. Wang, L. Huang, F. Pan, Y. Chen, B. Lei, M. Peng and M. Wu, *ACS Appl. Mater. Interfaces,* 2015, **7**, 10044.

10 M. M. Peng, X. W. Yin, P. A. Tanner, M. G. Brik and P. F. Li, *Chem. Mater.,* 2015, **27**, 2938.

11 Z. X. Qiu, T. T. Luo, J. L. Zhang, W. L. Zhou, L. P. Yu and S. X. Lian, *J. Lumin.,* 2015, **158**, 130.

12 R. P. Cao, M. M. Peng, E. H. Song and J. R. Qiu, *ECS J. Solid State. Sc.,* 2012, **1** (4), R123.

13 M. M. Peng, X.W. Yin, P. A. Tanner, C. Q. Liang, P. F. Li, Q. Y. Zhang and J. R. Qiu, *J. Am. Ceram. Soc.,* 2013, **96**, 2870.

14 D. Q. Chen, W. D. Xaing, X. J. Liang, J. S. Zhong, H. Yu, M. Y Ding, H. W. Lu and Z. G. Ji, *J. Euro. Ceram. Soc.*, 2015, **35**, 859.

15 R. Zhang, H. Lin, Y. L. Yu, D. Q. Chen, J. Xu and Y. S. Wang, *Laser Photonics Rev.,* 2014, **8**, 158.

16 L. A. Riseberg, M. J. Weber, *Solid State Commu.*, 1971, **9**, 791.

17 J. F. Donegan, T. J. Glynn, G. F. Imbusch, J. P. Remeika, *J. Lumin.*, 1986, **36**, 93.

18 L. H. Huang, C. Y. Wang, M. Q. Guo, Y. J. Hua, S. L. Zhao, D. G. Deng, H. P. Wang, G. H. Jia, X. Q. Xu, *Rare Metal Mater. Eng.*, 2012, **41**, 443.

19 M. G. Brik, S. J. Camardello and A. M. Srivastava, *ECS J. Solid State. Sc.,* 2014, **4**, R39.

20 P. F. Li, M. Y. Peng, X. W. Yin, Z. J. Ma, G. P. Dong, Q. Y. Zhang and J. R. Qiu, *Opt. Express,* 2013, **21**, 18943.

21 B. Wang, H. Lin, J. Xu, H. Chen and Y. S. Wang, *ACS Appl. Mater. Interfaces,* 2014, **6**, 22905.

22 T. Murata, T. Tanoue, M. Iwasaki, K. Morinaga and T. Hase, *J. Lumin.,* 2005, **114**, 207.

23 L. Wang, Y. D. Xu, D. Wang, R. L. Zhou, N. Ding, M. Shi, Y. Q. Chen, Y. Jiang and Y. H. Wang, *Phys. Status solidi. A,* 2013, **210**, 1433.

24 W. Shu, L. L Jiang, S. G Xiao, X. L Yang and J. W. Ding, *Mater. Sci. Eng. B,* 2012, **177**, 274.

25 J. Lu, Y. X. Pan, J. G. Wang, X. A. Chen, S. M. Huang and G. K. Liu, *RSC Adv.,* 2013, **3**, 4510.

26 Y. X. Pan and G. K. Liu, *J. Lumin.,* 2011, **131**, 465.

27 M. G. Brik, Y. X. Pan and G. K. Liu, *J. Alloys Compd.,* 2011, **509**, 1452.

28 L. L. Meng, L. F. Liang and Y. X. Wen, *J. Mater. Sci.,* 2014, **25**, 2676.

29 S. Bhushan and M. V. Chukichev, *J. Mater. Sci. Lett.,* 1988, **7**, 319.

30 L. L. Wei, C. C. Lin, M. H. Fang, M. G. Brik, S. F. Hu, H. Jiao and R. S. Liu, *J. Mater. Chem. C*, 2015, **3**, 1655.

31 D. Sekiguchi, J.-i. Nara and S. Adachi, *J. App. Phys.,* 2013, **113**, 183516.

32 D. Sekiguchi and S. Adachi, *ECS J. Solid State. Sc.,* 2014, **3**, R60.

33 Z. B. Lin, H. Lin, J. Xu, F. Huang, H. Chen, B. Wang and Y. S. Wang, *J. Alloys Compd.,* 2015, **649**, 661.

TOC

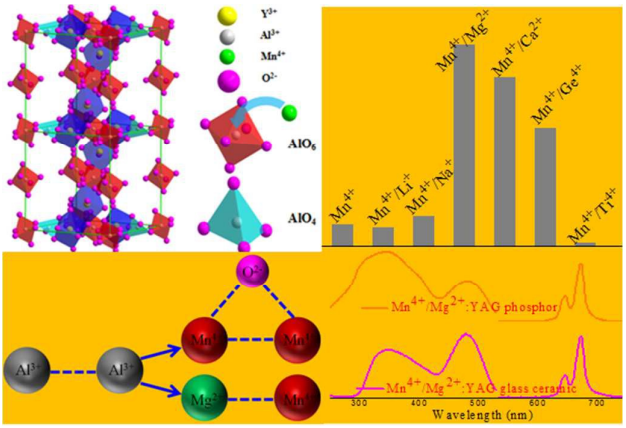

A non-rare-earth doped Mn^{4+}:$Y_3Al_5O_{12}$ red phosphor and the related glass-ceramics were fabricated to explore their application in white light-emitting diodes.